

# Geometrical Nonlinearity of Circular Plates and Membranes: an Alternative Method

D. Cattiaux\*, S. Kumar\*, X. Zhou\*\*, A. Fefferman\* and E. Collin\*,†

(\*) Univ. Grenoble Alpes, Institut Néel - CNRS UPR2940,

25 rue des Martyrs, BP 166, 38042 Grenoble Cedex 9, France

(\*\*) IEMN, Univ. Lille - CNRS UMR8520, Av. Henri Poincaré, Villeneuve d'Ascq 59650, France

(Dated: May 19, 2022)

We apply the well-established theoretical method developed for geometrical nonlinearities of micro/nano-mechanical beams to circular drums. The calculation is performed under *the same* hypotheses, the extra difficulty being to analytically describe the (coordinate-dependent) additional stress generated in the structure by the motion. An analytic expression is produced for the Duffing (hardening) nonlinear coefficient, which requires *only* the knowledge of the mode shape functions to be evaluated. This formulation, while lacking the rigor of the abundant literature on the subject, has the advantage of being comparatively much simpler; and does not rely ultimately on numerical methods. Moreover, no hypotheses are made on the drive scheme and the nature of the in-plane stress: it is not required to be of electrostatic origin. As a matter of illustration, we compare our predictions to two typical published experimental results: from a top-down (silicon-nitride) stressed micro-device and a bottom-up (graphene) unstressed nano-resonator. Generalization of the presented method to Duffing-type mode-coupling should be a straightforward extension of this work.

Keywords: Mechanics, Condensed Matter Physics, Nano-devices

## I. INTRODUCTION

The field of micro- and nano- electro-mechanics (MEMS and NEMS) [1–3] has been continuously expanding over the last decades. These devices, which transduce motion into electrical signals, have been both developed into sensors (e.g. pressure gauge [4]) and components (e.g. r.f. signal mixer [5]). Beyond the notorious accelerometer [6] and mass spectroscopy [7] applications, it even becomes possible today to embed nanomechanical elements into *quantum* electronic circuits [8–10].

Within the field, nonlinearities can be both a limitation or a *resource*. For all systems that build on linear response, nonlinearities of all kinds limit the dynamic range of the device [11]. On the other hand, one can devise efficient schemes that rely on nonlinearities to work: this very rich area includes applications such that e.g. amplification of small signals [12], bit storage [13, 14], and synchronization of oscillators [15, 16] among others.

In both cases, understanding and *mastering* the sources of nonlinearities is required, in order to tailor them on demand: maximizing, or minimizing them [17–19, 21]. The main feature that impacts the dynamics of MEMS/NEMS is a *Duffing-type* nonlinear behavior [20]. The basic modeling capturing the physics is a  $\hat{k}x^3$  restoring force inserted in the dynamics equation of the mechanical mode; in practice, other terms may also contribute and be taken into account [22].

Even if the materials are perfectly Hookean, all devices experience nonlinear behavior at large deformations: these arise from purely *geometrical* considerations. For flexural doubly-clamped beams, it consists of the extra stress stored in the beam under motion because of stretching [20]. This effect has been widely studied experimentally, even beyond the nonlinear features of a sin-

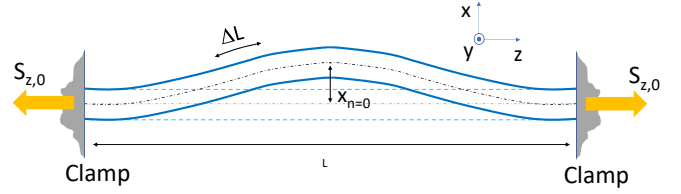


FIG. 1: (Color online) Schematic of a doubly-clamped device, in its fundamental flexure ( $n = 0$  mode). The axial force load  $S_{z,0}$  is here tensile.

gle mode: the same effect indeed couples all the flexural modes of the structure [23–25]. The measurements are in very good agreement with the simple theory built on arguments first proposed in Ref. [26]. As a matter of fact, this stretching modeling is a rather crude 1D description of actual devices, when compared to the literature that is rooted in continuum mechanics [27]. However, it has two undeniable qualities: it works, and it is *simple*.

For these reasons, we propose to extend this modeling to the 2D case of a drum. By no means shall this approach match the thoroughness of the extensive literature on the subject [28]. Our aim is rather to produce an *analytic, robust and simple* expression for the geometric nonlinear Duffing coefficient. This has to be contrasted with the conventional approach taken in the field, which reduces the problem to a system of coupled ordinary differential equations and ultimately relies on numerical methods [29, 30]. Besides, these recent works focus on the interplay between mechanics and electrostatic actuation; with the clear aim of fitting published experimental data [31]. On the other hand,

our modeling remains at a *generic level*, not introducing any specific drive fields. With no intention to be exhaustive, the validity of the presented result is assessed with a comparison to benchmark experimental results from the literature.

Let us start by recalling the basics of the geometrical nonlinear modeling of beams. We first write the Euler-Bernoulli equation that applies to thin-and-long structures [32]:

$$E_z I_z \frac{\partial^4 f(z, t)}{\partial z^4} + S_z \frac{\partial^2 f(z, t)}{\partial z^2} = -\rho A_z \frac{\partial^2 f(z, t)}{\partial t^2}, \quad (1)$$

with  $E_z$  the Young's modulus,  $I_z$  the second moment of area,  $S_z$  the axial force load,  $\rho$  the mass density and  $A_z$  the section area. The  $z$  index refers to the axis pointing along the beam, see Fig. 1. The beam is assumed homogeneous with a constant cross section over its length  $L$ . The function  $f(z, t)$  describes the transverse motion of the structure (in the  $x$  direction), with the proper boundary conditions. This equation essentially neglects rotational inertia of beam elementary elements  $\delta z$ , and *all shearing forces*.

When dealing with small displacements, Eq. (1) is solved by *linear superposition* of eigenmodes  $f_n(z, t)$ :

$$f_n(z, t) = x_n(t) \psi_n(z), \quad (2)$$

with  $\psi_n(z)$  the *mode shape* of mode  $n$  (no units), and corresponding mode resonance frequency  $\omega_n$ .  $x_n(t)$  is the time-dependent motion associated with the mode; by means of a Rotating-Frame Transform, it writes  $a_n(t) \cos(\omega t + \phi)$  with  $a_n(t)$  a slow varying amplitude variable, nonzero only for  $\omega \approx \omega_n$  (resonance condition). Here,  $S_z = S_{z,0} = \sigma_0 A_z$  the initially stored axial load in the structure (from uniaxial stress  $\sigma_0$ ). With this convention,  $S_z$  is negative for a *tensile* stored stress. Note that the quantitative value of  $x_n(t)$  depends on the normalization choice of  $\psi_n(z)$ ; in this paper we will always normalize modal functions to the maximum displacement amplitude, such that at this abscissa  $z_n$  one gets  $\psi_n(z_n) = 1$ .

The stretching of the beam writes  $S_z = S_{z,0} + \Delta S$  with  $|\Delta S| = E_z A_z \Delta L / L$  and  $\Delta L$  the extension [20]:

$$\Delta L = \frac{1}{2} \int_0^L \left( \frac{\partial f(z, t)}{\partial z} \right)^2 dz, \quad (3)$$

expanded at lowest order in  $f$ . Note that from Eq. (2) this expression is quadratic in motion amplitudes  $x_n(t)$ , thus a simple Rotating-Wave Approximation leads to an extension  $\Delta L \propto a_n^2 / 2$  (the slow variables): the nonlinear stretching is essentially a *static* effect, which is why there is no time-delay in the relationship between  $\Delta S$  and  $\Delta L$ .

The basic nonlinear modeling consists then in re-injecting Eq. (3) into Eq. (1), and *neglecting any other alterations due to the large motion amplitude*, e.g. higher

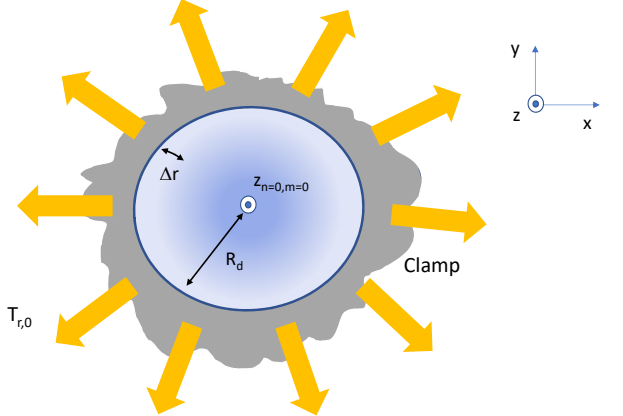


FIG. 2: (Color online) Schematic of a drum device, in its fundamental flexure ( $\{n = 0, m = 0\}$  mode). The biaxial force  $2\pi R_d T_{r,0}$  is here tensile.

order terms in the radius of curvature of the distorted shape or the modification of the mode shape  $\psi_n(z)$  itself [20, 26]. While the validity of these assumptions is questionable, it has been found experimentally that this modeling describes very well experimental results [23–25].

For a single mode  $f \rightarrow f_n$ , the projection of Eq. (1) onto it (i.e. multiplying the equation by  $\psi_n$  and integrating over the beam length) leads to the definition of *modal parameters*:

$$m_n = \rho A_z \int_0^L [\psi_n(z)]^2 dz, \quad (4)$$

$$k_n = E_z I_z \int_0^L \left[ \frac{d^2 \psi_n(z)}{dz^2} \right]^2 dz - S_{z,0} \int_0^L \left[ \frac{d \psi_n(z)}{dz} \right]^2 dz, \quad (5)$$

$$\tilde{k}_n = \frac{E_z A_z}{2 L} \left( \int_0^L \left[ \frac{d \psi_n(z)}{dz} \right]^2 dz \right)^2, \quad (6)$$

with  $m_n$  the mode mass,  $k_n$  the mode spring constant and  $\tilde{k}_n$  the Duffing nonlinear parameter. The resonance frequency verifies  $\omega_n = \sqrt{k_n / m_n}$ . Including in Eq. (1) a damping and a drive term is straightforward [20]. The obtained equation of motion for  $x_n$  is then the one of a harmonic oscillator plus a *purely cubic nonlinear restoring term*  $+\tilde{k}_n x_n(t)^3$ .  $\tilde{k}_n$  is always positive, because of stretching (the mode “hardens”); in the steady-state ( $a_n = \text{constant}$ ), the resonant response measured while sweeping the drive frequency upwards will be *pulled up*, with the frequency at maximum amplitude  $a_n^{\max}$  given by  $\omega_n^{\text{res}} = \omega_n + \beta_n (a_n^{\max})^2$  with  $\beta_n = \frac{3}{8} \omega_n \frac{\tilde{k}_n}{k_n}$  [20, 22]. The free-decay solution can also be analytically produced [22]. Owing to the success of this modeling, we present below its exact analog in two dimensions.

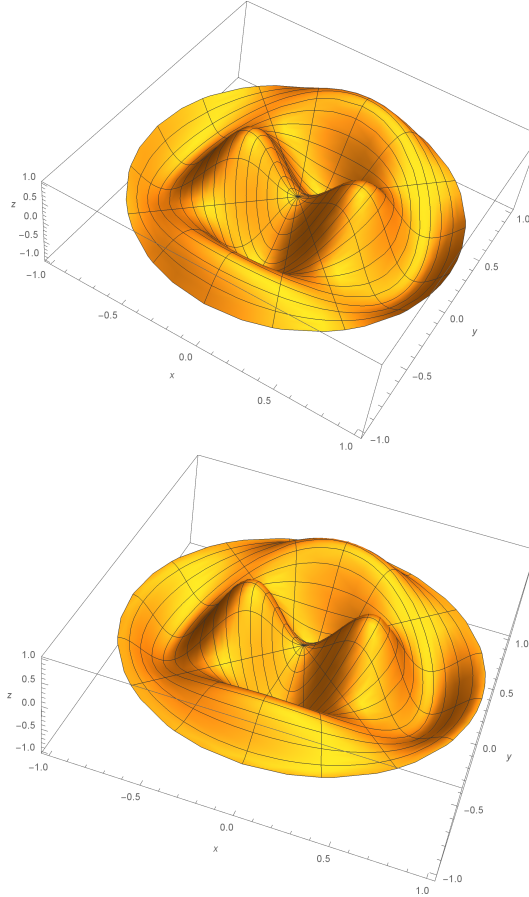


FIG. 3: (Color online) Calculated mode shape  $\psi_{n,m}(r, \theta)$  for mode  $\{n = 2, m = 1\}$  (radius  $R_d = 1$ ). Top: high-stress limit. Bottom: low-stress limit. Both are very similar in topography.

## II. FORMULATION OF THE PROBLEM

We now develop the same ideas for the case of a 2D circular structure, see Fig. 2. We first remind the reader about the conventional *linear* theory [3]. The generic formalism applying to thin drums [obtained within the same reasoning as Eq. (1)] is the Kirchhoff-Love equation:

$$D_r \Delta^2 f(r, \theta, t) + T_{r,0} \Delta f(r, \theta, t) = -\rho h \frac{\partial^2 f(r, \theta, t)}{\partial t^2}, \quad (7)$$

with  $\Delta \cdots = \frac{1}{r} \frac{\partial}{\partial r} (r \frac{\partial \cdots}{\partial r}) + \frac{1}{r^2} \frac{\partial^2 \cdots}{\partial \theta^2}$  the Laplacian operator (here in polar coordinates),  $D_r = \frac{1}{12} E_r h^3 / (1 - \nu_r^2)$  the flexural rigidity in the plane of the drum ( $\nu_r$  being Poisson's ratio),  $2\pi R_d T_{r,0} = 2\pi R_d h \sigma_0$  the tension within the drum,  $h$  its thickness and  $R_d$  its radius. We assume materials properties  $E_r, \nu_r, \rho, \sigma_0$  and thickness  $h$  to be homogeneous and isotropic over the device; in Eq. (7), the  $T_{r,0}$  term resulting from the biaxial stress  $\sigma_0$  is taken negative for *tensile* load.

In the limit of small displacements, we write:

$$f_{n,m}(r, \theta, t) = z_{n,m}(t) \psi_{n,m}(r, \theta), \quad (8)$$

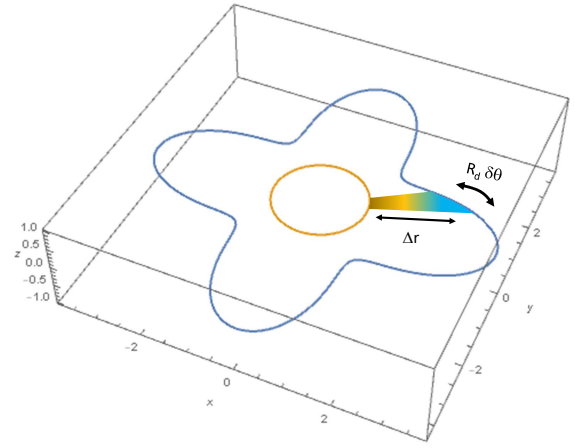


FIG. 4: (Color online) Normalized stretching function  $\epsilon$  plotted for mode  $\{n = 2, m = 1\}$  in high-stress limit (with  $z_{n,m}/R_d = 1$ ). The stretched surface area  $R_d \delta \theta \Delta r$  is indicated on the graph (central circle represents the drum).

with  $\psi_{n,m}(r, \theta) = \phi_{n,m}(r) \cos(n\theta)$  the mode shapes and  $z_{n,m}(t)$  the motion amplitude; now two indexes are necessary to label all 2D flexural modes of the structure. Two simple limits are considered in this paper: the high-stress case (membranes,  $D_r = 0$  with  $T_{r,0} < 0$  here), and the low-stress one (plates,  $T_{r,0} = 0$ ). Using the boundary conditions, the solutions write:

$$\phi_{n,m}(r) = \frac{\text{BesselJ}_n\left(\frac{\lambda_{n,m} r}{R_d}\right)}{\text{BesselJ}_n\left(\frac{\lambda_{n,m} r_{n,m}}{R_d}\right)},$$

or

$$\frac{\text{BesselI}_n\left(\frac{\lambda_{n,m} r}{R_d}\right) - \frac{\text{BesselI}_n(\lambda_{n,m})}{\text{BesselJ}_n(\lambda_{n,m})} \text{BesselJ}_n\left(\frac{\lambda_{n,m} r}{R_d}\right)}{\text{BesselI}_n\left(\frac{\lambda_{n,m} r_{n,m}}{R_d}\right) - \frac{\text{BesselI}_n(\lambda_{n,m})}{\text{BesselJ}_n(\lambda_{n,m})} \text{BesselJ}_n\left(\frac{\lambda_{n,m} r_{n,m}}{R_d}\right)},$$

for high-stress and low-stress respectively.  $\lambda_{n,m}$  is the mode parameter and  $r_{n,m}$  the radial position of the maximum amplitude (occurring for given angles  $\theta$  when  $n \neq 0$ ). We give the first modes  $\lambda_{n,m}$  and  $r_{n,m}$  in Tab. I (Appendix A); the mode  $\{n = 2, m = 1\}$  is displayed as an example in Fig. 3 for the two limits (top: high-stress, bottom: low-stress).

The stretching in 2D is a *change of surface area per unit angle*. This writes mathematically:

$$\frac{\delta S}{\delta \theta} = \frac{1}{2} \int_0^{R_d} \left[ \left( \frac{\partial f(r, \theta, t)}{\partial r} \right)^2 + \frac{1}{r^2} \left( \frac{\partial f(r, \theta, t)}{\partial \theta} \right)^2 \right] r dr, \quad (10)$$

at lowest order in  $f$ . Geometrically, this quantity is

directly linked to the *radial* strain  $\epsilon = \Delta r/R_d$  experienced by the drum at its edge:  $\delta S = R_d \delta \theta \Delta r$ , i.e.  $\frac{\delta S(\theta, t)}{\delta \theta} = R_d^2 \epsilon(\theta, t)$  [see Fig. 4]. Injecting the mode shape Eq. (8) into Eq. (10), one obtains:

$$\epsilon(\theta, t) = \left( \frac{z_{n,m}(t)}{R_d} \right)^2 \times \left[ \frac{C_{n,m}^{(1)} + C_{n,m}^{(2)}}{2} + \frac{C_{n,m}^{(1)} - C_{n,m}^{(2)}}{2} \cos(2n\theta) \right], \quad (11)$$

where we have defined (constants with no dimensions):

$$C_{n,m}^{(1)} = \frac{1}{2} \int_0^{R_d} \left( \frac{d\phi_{n,m}(r)}{dr} \right)^2 r dr, \quad (12)$$

$$C_{0,m}^{(2)} = C_{0,m}^{(1)}, \quad (13)$$

$$C_{n,m}^{(2)} = \frac{1}{2} \int_0^{R_d} \frac{n^2}{r^2} \phi_{n,m}(r)^2 r dr \text{ for } n \neq 0.$$

The  $C_{n,m}^{(1,2)}$  constants of the first modes are given in Tab. IV, Appendix C. We omit indexes  $n, m$  in the labeling of  $\epsilon$  for simplicity. The function Eq. (11) is plotted in Fig. 4 for mode  $\{n = 2, m = 1\}$  in the high-stress limit.

For  $n = 0$ , the problem is isotropic and the solution rather straightforward. However for  $n \neq 0$ , the stress within the drum *has an extra angle-dependent component*  $\cos(2n\theta)$ . Eq. (7) has thus to be modified to:

$$\begin{aligned} & D_r \Delta^2 f \\ & + \int_{-h/2}^{+h/2} \frac{1}{r} \frac{\partial}{\partial r} \left( \sigma_r r \frac{\partial f}{\partial r} \right) + \frac{1}{r^2} \frac{\partial}{\partial \theta} \left( \sigma_\theta \frac{\partial f}{\partial \theta} \right) dz \\ & = -\rho h \frac{\partial^2 f}{\partial t^2}, \end{aligned} \quad (14)$$

with  $\sigma_r(r, \theta, z, t), \sigma_\theta(r, \theta, z, t)$  the superposition of the initial biaxial stress  $\sigma_0$  *plus* the elastic response of the drum to the strain  $\epsilon$ , Eq. (11). These stress components are defined below. As for beams, we neglect any other nonlinear contribution arising from the large motion amplitude; shear stresses (e.g.  $\sigma_{r,\theta}$  component) are not taken into account in Kirchhoff-Love theory (as in Euler-Bernoulli).

### III. STRESS FIELD

The next step is thus to compute the stress field within the device; this is indeed the extra difficulty that arises in 2D. As for beams, we assume that the stretching is adiabatic, i.e. the stress/strain relation can be treated in a time-independent manner. The total stress field is the sum of a *homogeneous* contribution, plus the response to the *angle-dependent* stretching. The former is straight-

forward (e.g. Appendix B):

$$\sigma_r^{hom.} = \sigma_0 - E_r \frac{1}{1 - \nu_r} \epsilon^{hom.}, \quad (15)$$

$$\sigma_\theta^{hom.} = \sigma_0 - E_r \frac{1}{1 - \nu_r} \epsilon^{hom.}, \quad (16)$$

$$\sigma_z^{hom.} = 0, \quad (17)$$

with all shears equal to zero  $\sigma_{r,z} = \sigma_{r,\theta} = \sigma_{\theta,z} = 0$ . The  $-$  sign above comes from our stress convention. In the problem at stake, from Eq. (11) we have  $\epsilon^{hom.} = \left( \frac{z_{n,m}}{R_d} \right)^2 \left[ \frac{C_{n,m}^{(1)} + C_{n,m}^{(2)}}{2} \right]$ . This stress field component remains *biaxial*.

To compute the angle-dependent term, we start with an *ansatz* for the associated displacement field  $\{u_r, u_\theta, u_z\}$ :

$$u_r = R_d f_r(r, z) \epsilon^{angl.}(\theta), \quad (18)$$

$$u_\theta = R_d f_\theta(r, z) \frac{d\epsilon^{angl.}(\theta)}{d\theta}, \quad (19)$$

$$u_z = h f_z(r, z) \epsilon^{angl.}(\theta), \quad (20)$$

with  $\epsilon^{angl.} = \left( \frac{z_{n,m}}{R_d} \right)^2 \left[ \frac{C_{n,m}^{(1)} - C_{n,m}^{(2)}}{2} \cos(2n\theta) \right]$ . These expressions are then injected in the well-known *equilibrium equations* of elasticity theory (see e.g. [2]), neglecting inertial terms; these are given for the interested reader in Appendix B.

Introducing reduced variables  $\tilde{r} = r/R_d$  and  $\tilde{z} = z/h$ , one can show that the displacement functions have to be written, at lowest order in  $h/R_d \ll 1$  (thin structure):

$$f_r(\tilde{r}, \tilde{z}) = c_r(\tilde{r}) |\tilde{z}| + b_r(\tilde{r}) + a_r(\tilde{r}) (\tilde{z})^2 \left[ \frac{h}{R_d} \right]^2, \quad (21)$$

$$f_\theta(\tilde{r}, \tilde{z}) = c_\theta(\tilde{r}) |\tilde{z}| + b_\theta(\tilde{r}) + a_\theta(\tilde{r}) (\tilde{z})^2 \left[ \frac{h}{R_d} \right]^2, \quad (22)$$

$$\begin{aligned} f_z(\tilde{r}, \tilde{z}) &= c_z(\tilde{r}) |\tilde{z}| + b_z(\tilde{r}) + a_z(\tilde{r}) (\tilde{z})^2 \left[ \frac{h}{R_d} \right]^2 \\ &- \frac{1}{4(1 - \nu_r)} \left( \frac{c_r(\tilde{r}) - (2n)^2 c_\theta(\tilde{r}) + \tilde{r} \frac{dc_r(\tilde{r})}{d\tilde{r}}}{\tilde{r}} \right) (\tilde{z})^2. \end{aligned} \quad (23)$$

For the nine (adimensional) functions  $a_X, b_X, c_X$  ( $X = r, \theta, z$ ) of the  $\tilde{r}$ -variable, we then chose the following *ansatz*:

$$b_r(\tilde{r}) = b_{r,0} \tilde{r}^\alpha, \quad (24)$$

$$b_\theta(\tilde{r}) = b_{\theta,0} \tilde{r}^\alpha, \quad (25)$$

$$c_r(\tilde{r}) = c_{r,0} \tilde{r}^\alpha, \quad (26)$$

$$c_\theta(\tilde{r}) = c_{\theta,0} \tilde{r}^\alpha, \quad (27)$$

$$b_z(\tilde{r}) = b_{z,0} \tilde{r}^{\alpha-1}, \quad (28)$$

$$c_z(\tilde{r}) = c_{z,0} \tilde{r}^{\alpha-1}, \quad (29)$$

$$a_r(\tilde{r}) = a_{r,0} \tilde{r}^{\alpha-2}, \quad (30)$$

$$a_\theta(\tilde{r}) = a_{\theta,0} \tilde{r}^{\alpha-2}, \quad (31)$$

and:

$$a_z(\tilde{r}) = a_{z,0} \tilde{r}^{\alpha-3}, \quad (32)$$

which leads to seven equations linking the above introduced constants. Obviously,  $\alpha \geq 3$  to guarantee a physical solution.

Three more equations are obtained from the stress boundary conditions on the surface of the drum:  $\sigma_z(r, \theta, z = \pm h/2) = 0$ ,  $\sigma_{r,z}(r, \theta, z = \pm h/2) = 0$  and  $\sigma_{\theta,z}(r, \theta, z = \pm h/2) = 0$ . The last relation is obtained from the stretching on the periphery, equating the radial strain  $\partial u_r / \partial r$  to  $\epsilon^{angl.}$  at  $r = R_d$  (see Fig. 4). Solving the problem under Mathematica<sup>®</sup>, we list the constants appearing in Eqs. (25-32) in Tab. II, Appendix B (as a function of  $n$  and  $\nu_r$ ). The exponent  $\alpha$  is found to be  $2n + 1$ , reminding  $n \neq 0$ .

The  $\theta$ -dependent stress field can finally be calculated. The normal components write, in the limit  $h/R_d \approx 0$ :

$$\sigma_r^{angl.} = -E_r \eta_r^{(n)}(\nu_r) \left( \frac{r}{R_d} \right)^{\alpha-1} \epsilon^{angl.}, \quad (33)$$

$$\sigma_\theta^{angl.} = -E_r \eta_\theta^{(n)}(\nu_r) \left( \frac{r}{R_d} \right)^{\alpha-1} \epsilon^{angl.}, \quad (34)$$

$$\sigma_z^{angl.} = 0. \quad (35)$$

The functions  $\eta_r^{(n)}(\nu_r)$  and  $\eta_\theta^{(n)}(\nu_r)$  with  $n \neq 0$  are defined by:

$$\eta_r^{(n \neq 0)}(\nu_r) = \frac{1 + 2n - 2(1 + n)\nu_r}{(1 + 2n)(1 + \nu_r)}, \quad (36)$$

$$\eta_\theta^{(n \neq 0)}(\nu_r) = -\frac{3 + 4n}{(1 + 2n)(1 + \nu_r)}. \quad (37)$$

The only nonzero shear stress is  $\sigma_{r,\theta}$  (see Appendix B). It shall be neglected in this modified Kirchhoff-Love theory, as already stated. As an example, the computed (normalized) stress components are displayed in Fig. 5 for mode  $\{n = 2, m = 1\}$ , in the high-stress limit.

Angle-dependent terms Eqs. (33-35) and homogeneous terms Eqs. (15 -17) can be rewritten in a compact form:

$$\sigma_r = \sigma_0 - E_r \left[ \eta_r^{(0)}(\nu_r) \epsilon^{hom.} + \eta_r^{(n)}(\nu_r) \left( \frac{r}{R_d} \right)^{2n} \epsilon^{angl.} \right], \quad (38)$$

$$\sigma_\theta = \sigma_0 - E_r \left[ \eta_\theta^{(0)}(\nu_r) \epsilon^{hom.} + \eta_\theta^{(n)}(\nu_r) \left( \frac{r}{R_d} \right)^{2n} \epsilon^{angl.} \right], \quad (39)$$

$$\sigma_z = 0, \quad (40)$$

provided we define  $\eta_r^{(0)}(\nu_r) = \eta_\theta^{(0)}(\nu_r) = \eta^{(0)}(\nu_r) = 1/(1 - \nu_r)$ . The stress is still *planar*, and independent of  $z$ , but  $\sigma_r \neq \sigma_\theta$  and is neither homogeneous nor isotropic. Injecting these in Eq. (14), we can now solve the problem at hand.

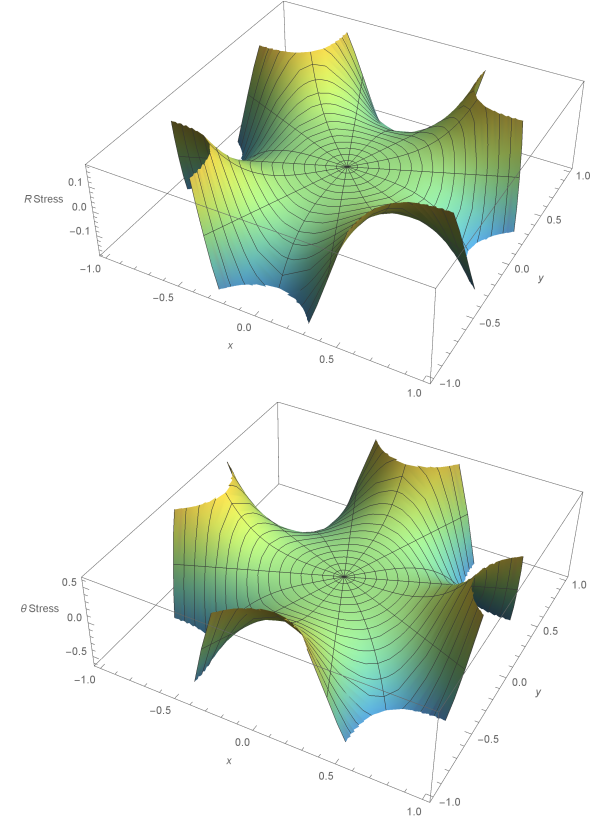


FIG. 5: (Color online) Stress components  $\sigma_r^{angl.}$  (top) and  $\sigma_\theta^{angl.}$  (bottom) computed for mode  $\{n = 2, m = 1\}$  in the high-stress limit. The graph has been normalized to  $E_r = 1$ ,  $R_d = 1$ , and  $z_{n,m}/R_d = 1$  (using  $\nu_r = +0.3$ ).

#### IV. MODE PARAMETERS

Having found the stress field, we can now project Eq. (14) on a given mode  $\{n, m\}$ . We thus define modal parameters:

$$\mathcal{M}_{n,m} = \rho h \int_0^{2\pi} \int_0^{R_d} [\psi_{n,m}(r, \theta)]^2 r dr d\theta, \quad (41)$$

$$\begin{aligned} \mathcal{K}_{m,n} = D_r \int_0^{2\pi} \int_0^{R_d} & [\psi_{n,m}(r, \theta) \Delta^2 \psi_{n,m}(r, \theta)] r dr d\theta \\ & + T_{r,0} \int_0^{2\pi} \int_0^{R_d} [\psi_{n,m}(r, \theta) \Delta \psi_{n,m}(r, \theta)] r dr d\theta, \end{aligned} \quad (42)$$

in a similar fashion to Eqs. (4 - 5). The resonance frequencies  $\omega_{n,m} = \sqrt{\mathcal{K}_{m,n}/\mathcal{M}_{n,m}}$  reduce to:

$$\begin{aligned} \omega_{n,m} = & \sqrt{\frac{|T_{r,0}|}{\rho h}} \left( \frac{\lambda_{n,m}}{R_d} \right) \\ \text{or} \\ & \sqrt{\frac{D_r}{\rho h}} \left( \frac{\lambda_{n,m}}{R_d} \right)^2, \end{aligned} \quad (43)$$

in the limit of high-stress and low-stress devices, respectively. We give mass and spring values for the first modes in Tab. III, Appendix C.

Beyond the usual linear coefficients, the Duffing term analogous to Eq. (6) finally writes:

$$\begin{aligned} \tilde{\mathcal{K}}_{n,m} = & -\frac{E_r h}{R_d^2} \times & (44) \\ & \left[ \frac{C_{n,m}^{(1)} + C_{n,m}^{(2)}}{2} \eta^{(0)}(\nu_r) \int_0^{2\pi} \int_0^1 [\psi_{n,m}(\tilde{r}, \theta) \Delta \psi_{n,m}(\tilde{r}, \theta)] \tilde{r} d\tilde{r} d\theta \right. \\ & + \frac{C_{n,m}^{(1)} - C_{n,m}^{(2)}}{2} \times \\ & \left( \eta_r^{(n)}(\nu_r) \frac{\pi}{2} \int_0^1 \frac{\phi_{n,m}(\tilde{r})}{\tilde{r}} \frac{d}{d\tilde{r}} \left( \tilde{r}^{2n+1} \frac{d\phi_{n,m}(\tilde{r})}{d\tilde{r}} \right) \tilde{r} d\tilde{r} \right. \\ & \left. + \eta_\theta^{(n)}(\nu_r) \frac{n^2 \pi}{2} \int_0^1 \frac{\tilde{r}^{2n+1} \phi_{n,m}(\tilde{r})^2}{\tilde{r}^3} \tilde{r} d\tilde{r} \right) \right], \end{aligned}$$

with the integrals written in normalized units  $\tilde{r} = r/R_d$  (no dimensions).

Numerical values for the integrals defining the coefficients  $\tilde{\mathcal{K}}_{n,m}$  are listed and discussed for the first modes in Appendix C, Tabs. V and VI. For beams, Eq. (6) leads to a scaling of the Duffing parameter  $\tilde{k}_n \propto E_z A_z / L^3$ . Similarly here, Eq. (44) leads to  $\tilde{\mathcal{K}}_{n,m} \propto E_r (h 2\pi R_d) / R_d^3$ ; in both cases, the Duffing effect is a *stiffening*.

## V. CONCLUSION

Following the same methodology as for beams, we present a theory describing the geometrical (stretching) nonlinearity of drum devices. The basic hypotheses are to neglect any other nonlinear features apart from the extra tensile stress, to neglect shearing forces, and to treat the stretching as a static effect. Two limits are considered for numerical estimates: high-stress (membranes) and low-stress (plates), but the mathematical description is written in a generic fashion. The difficulty lies in the calculation of the stress profile induced in the stretched drum for non-axisymmetric modes; the analytic solution however exists in the limit of a thin structure.

As for beams, the approach presented *is not* intended to match the rigorous treatments that can be found in the literature on mechanical nonlinearities. However, building on the great success of the beam stretching description, it presents an alternative, *simple and fully analytic* modeling of the Duffing nonlinear response of plates and membranes. Only the knowledge of the mode shapes is necessary for the calculation of the Duffing coefficient, through simple integrals evaluation. This is by far more tractable than the numerical treatments that are required in the standard mechanical engineering theories.

In order to illustrate the validity of the approach, we can compare the theory to benchmark experimental data published for modes  $\{n = 0, m = 0\}$ . A full comparison

of the presented model to more elaborate nonlinear theories is out of the scope of the present work; as for the beam stretching approach, this is a subject on its own that shall be published elsewhere. In Ref. [34] the nonlinear behavior of a square silicon nitride drum has been studied. From Fig. 1 (b) of this article, we infer a Duffing parameter normalized to the mode mass of about  $\tilde{\mathcal{K}}_{0,0}/\mathcal{M}_{0,0} \approx +1.5 \cdot 10^{23} \text{ m}^2/\text{s}^2$ . This fits the data for weak enough excitations; with larger drives, other nonlinear features kick in [34]. Even though the initial stress  $\sigma_0$  stored in the structure is not very high (110 MPa), the device is well within the *membrane* limit. From the parameters given in the publication (supplementary material,  $E_r = 240 \text{ GPa}$ ,  $\rho = 3200 \text{ kg/m}^3$ , thickness  $h = 480 \text{ nm}$ ), taking a standard Poisson ratio of  $\nu_r = +0.3$  and approximating the first mode by a circular shape of radius  $R_d \approx 210 \mu\text{m}$  [consistent with Fig. 2 (a)] which should be enough for the purpose of our illustration here, we obtain  $\tilde{\mathcal{K}}_{0,0}/\mathcal{M}_{0,0} \approx +1.2 \cdot 10^{23} \text{ m}^2/\text{s}^2$ . The corresponding mode resonance frequency calculated is 338 kHz, matching also consistently the measured 321 kHz.

In Ref. [33] the nonlinear behavior of a (multilayer) graphene drum has been studied. The reported stored stress is very low (about 5 MPa), and the device is better described in the *plate* limit. From parameters quoted in the publication ( $E_r \approx 700 \text{ GPa}$ ,  $\rho = 600 \text{ kg/m}^3$ ,  $R_d = 2.5 \mu\text{m}$ ,  $h = 5 \text{ nm}$ , neglecting the Poisson ratio) we compute  $\tilde{\mathcal{K}}_{0,0}/\mathcal{M}_{0,0} \approx +3.3 \cdot 10^{31} \text{ m}^2/\text{s}^2$  for a resonance frequency of 12.8 MHz. Again, this is in close agreement with measured values of  $+2 \cdot 10^{31} \text{ m}^2/\text{s}^2$  and 14.5 MHz respectively, given for the zero DC voltage bias limit.

As for beams, the proposed modeling seems to reproduce rather well experimental data. Further comparison should be done with higher modes, especially non-axisymmetric ones ( $n \neq 0$ ). Besides, the presented theory can be in principle extended to mode-coupling [23, 24]; an experimental and theoretical study of this regime would definitely assess the validity of the presented mathematical methods.

Data sharing is not applicable to this article as no new data were created or analyzed in this study.

(†) Corresponding Author: eddy.collin@neel.cnrs.fr

## Acknowledgments

We acknowledge support from the ERC CoG grant ULT-NEMS No. 647917, StG grant UNIGLASS No. 714692 and the STaRS-MOC project from *Région Hauts-de-France*. The research leading to these results has received funding from the European Union's Horizon 2020 Research and Innovation Programme, under grant agreement No. 824109, the European Microkelvin Platform (EMP).

## Appendix A: Mode parameters

In the Table below we give the first modes  $\lambda_{n,m}$  and  $r_{n,m}$  parameters for both high-stress (H.S.) and low-stress (L.S.) limits. Inserting these in Eqs. (9) one can easily compute the corresponding mode shapes (see Fig. 3 for an example).

mode $\{n, m\}$	H.S. $\lambda_{n,m}$	H.S. $r_{n,m}$	L.S. $\lambda_{n,m}$	L.S. $r_{n,m}$
$\{0, 0\}$	2.40483	0.	3.19622	0.
$\{0, 1\}$	5.52008	0.	6.30644	0.
$\{1, 0\}$	3.83171	0.4805123	4.61090	0.4102482
$\{1, 1\}$	7.01559	0.2624418	7.79927	0.2358243
$\{0, 2\}$	8.65373	0.	9.43950	0.
$\{2, 0\}$	5.13562	0.5947163	5.90568	0.5258299
$\{1, 2\}$	10.1735	0.1809784	10.9581	0.1680282
$\{2, 1\}$	8.41724	0.3628549	9.19688	0.3319174
...	...	...	...	...

TABLE I: First mode parameters. Left: high-stress (H.S.), right: low-stress (L.S.). For  $n = 0$  modes, the maximum amplitude is at the center ( $r_{0,m} = 0$ ).

## Appendix B: Stress field solution

We remind the reader basics of elasticity theory expressed in cylindrical coordinates. The strain fields can be written in terms of the displacement fields:

$$\begin{aligned}\epsilon_r &= \frac{\partial u_r}{\partial r}, \\ \epsilon_\theta &= \frac{u_r}{r} + \frac{1}{r} \frac{\partial u_\theta}{\partial \theta}, \\ \epsilon_z &= \frac{\partial u_z}{\partial z},\end{aligned}$$

for the normal components, and:

$$\begin{aligned}2\epsilon_{r,\theta} &= \frac{\partial u_\theta}{\partial r} - \frac{u_\theta}{r} + \frac{1}{r} \frac{\partial u_r}{\partial \theta}, \\ 2\epsilon_{r,z} &= \frac{\partial u_r}{\partial z} + \frac{\partial u_z}{\partial r}, \\ 2\epsilon_{\theta,z} &= \frac{1}{r} \frac{\partial u_z}{\partial \theta} + \frac{\partial u_\theta}{\partial z},\end{aligned}$$

for the shear strains.

For an isotropic homogeneous Hookean material, we have:

$$\begin{pmatrix} \sigma_r \\ \sigma_\theta \\ \sigma_z \\ \sigma_{r,\theta} \\ \sigma_{r,z} \\ \sigma_{\theta,z} \end{pmatrix} = \frac{E_r}{(1 + \nu_r)(1 - 2\nu_r)} (\mathcal{H}) \begin{pmatrix} \epsilon_r \\ \epsilon_\theta \\ \epsilon_z \\ 2\epsilon_{r,\theta} \\ 2\epsilon_{r,z} \\ 2\epsilon_{\theta,z} \end{pmatrix}$$

with  $(\mathcal{H}) =$

$$\begin{pmatrix} 1 - \nu_r & \nu_r & \nu_r & 0 & 0 & 0 \\ \nu_r & 1 - \nu_r & \nu_r & 0 & 0 & 0 \\ \nu_r & \nu_r & 1 - \nu_r & 0 & 0 & 0 \\ 0 & 0 & 0 & \frac{1-2\nu_r}{2} & 0 & 0 \\ 0 & 0 & 0 & 0 & \frac{1-2\nu_r}{2} & 0 \\ 0 & 0 & 0 & 0 & 0 & \frac{1-2\nu_r}{2} \end{pmatrix}$$

for the relationship between stresses ( $\sigma$ ) and strains ( $\epsilon$ ).

The equilibrium equations then write:

$$\begin{aligned}\frac{\partial \sigma_r}{\partial r} + \frac{1}{r} \frac{\partial \sigma_{r,\theta}}{\partial \theta} + \frac{1}{r} (\sigma_r - \sigma_\theta) + \frac{\partial \sigma_{r,z}}{\partial z} &= 0, \\ \frac{\partial \sigma_{r,\theta}}{\partial r} + \frac{1}{r} \frac{\partial \sigma_\theta}{\partial \theta} + 2 \frac{\sigma_{r,\theta}}{r} + \frac{\partial \sigma_{\theta,z}}{\partial z} &= 0, \\ \frac{\partial \sigma_{r,z}}{\partial r} + \frac{1}{r} \frac{\partial \sigma_{\theta,z}}{\partial \theta} + \frac{\sigma_{r,z}}{r} + \frac{\partial \sigma_z}{\partial z} &= 0,\end{aligned}$$

when neglecting the inertial terms.

The solution for the *homogeneous* stretching component is straightforward. The well-known displacement field simply writes:

$$\begin{aligned}f_r(r, z) &= r, \\ f_\theta(r, z) &= 0, \\ f_z(r, z) &= -\frac{2\nu_r}{1 - \nu_r} z,\end{aligned}$$

with  $u_r = f_r \epsilon^{hom.}$ ,  $u_\theta = 0$ ,  $u_z = f_z \epsilon^{hom.}$  by definition. Then  $\epsilon_r = \epsilon_\theta = \epsilon^{hom.}$  and  $\epsilon_z = -2\nu_r \epsilon^{hom.} / (1 - \nu_r)$ ; all other components of the strain field are zero. Clearly, imposing a radial stretching also causes *nonzero tangential and vertical strains*. The resulting stresses are Eqs. (15-17).

The case of the angular-dependent component is much more complex. Injecting in the above the *ansatz* Eqs. (18-20) for the displacement fields, and writing the problem in reduced coordinates, we realize that the solution should be of the type Eqs. (21-23) at lowest order in  $h/R_d$ . The symmetry of the drum with respect to  $z \rightarrow -z$  has been used. To further reduce the problem, another *ansatz* is needed for the  $\tilde{r}$ -dependent functions introduced in the writing of the solution: we assume them to be power laws, Eqs. (25-32). Taking into account the boundary conditions (no  $z$ -component stress on the surface of the drum, and fixed radial strain at the periphery), we end up with the constants listed in Tab. II.

The  $\epsilon_0$  term is simply the prefactor of the angular-dependent strain,  $\epsilon^{angl.} = \epsilon_0 \cos(2n\theta)$ . The stresses do depend on  $\tilde{z}^2$ . However, in the limit  $h/R_d \rightarrow 0$  these terms vanish and the stress components are homogeneous within the thickness of the drum. Also  $\sigma_z = 0$ : the stress state is *planar*. The two normal components  $\sigma_r^{angl.}, \sigma_\theta^{angl.}$  Eqs. (33-34) are displayed in Fig. 5 for mode  $\{n = 2, m = 1\}$  in the high-stress limit.

Furthermore, the only nonzero shear stress component

is  $\sigma_{r,\theta}^{angl.}$ . It then writes:

$$\sigma_{r,\theta}^{angl.} = -E_r \frac{n(-3 + \nu_r) + (-2 + \nu_r)}{(1 + 2n)(1 + \nu_r)} \left( \frac{r}{R_d} \right)^{2n} \epsilon_0 \sin(2n\theta),$$

with the  $-$  sign matching our stress convention (tensile). It is neglected in the presented modeling.

Parameter	Expression
$b_{r,0}$	$\epsilon_0/(1 + 2n)$
$b_{\theta,0}$	$b_{r,0} 2(1 + n)(2 - \nu_r)/(2n)^2$
$c_{r,0}$	0
$c_{\theta,0}$	0
$b_{z,0}$	0
$c_{z,0}$	$b_{r,0} 2(1 + n)\nu_r$
$a_{r,0}$	$-b_{r,0} 2[(1 + n)(2 - \nu_r) - n^2]$
$a_{\theta,0}$	$b_{r,0} n[1 - 4(1 + n)(2 - \nu_r)/(2n)^2]$
$a_{z,0}$	0
$\alpha$	$2n + 1$
$\epsilon_0$	$\left( \frac{z_{n,m}}{R_d} \right)^2 \frac{C_{n,m}^{(1)} - C_{n,m}^{(2)}}{2}$

TABLE II: Strain coefficients of the angular-dependent contribution, as a function of  $n, \nu_r$ .  $\epsilon_0$  is the amplitude of the  $\cos(2n\theta)$  stretching term.

### Appendix C: Mass, spring and Duffing parameters

In this Appendix we give numerical estimates for mass, spring constant and nonlinear parameters calculated for the first modes, in the two simple limits of high-stress and low-stress.

mode $\{n, m\}$	H.S. $M_{n,m}$	H.S. $K_{n,m}$	L.S. $M_{n,m}$	L.S. $K_{n,m}$
$\{0, 0\}$	0.269513	0.779325	0.182834	9.54057
$\{0, 1\}$	0.115780	1.763983	0.101896	80.5872
$\{1, 0\}$	0.239561	1.758616	0.184581	41.7156
$\{1, 1\}$	0.133016	3.273413	0.119933	221.883
$\{0, 2\}$	0.073686	2.759075	0.067543	268.132
$\{2, 0\}$	0.243735	3.214208	0.200046	121.669
$\{1, 2\}$	0.092082	4.765268	0.085466	616.168
$\{2, 1\}$	0.155586	5.511635	0.142446	509.546
...	...	...	...	...

TABLE III: Mass and spring constant for the first modes (norm. integrals, see text). Left: high-stress (H.S.) and right: low-stress (L.S.).

For this purpose, we re-write the relevant integrals in an adimensional form such that:

$$\mathcal{M}_{n,m} = \rho h \pi R_d^2 M_{n,m},$$

and:

$$\begin{aligned} \mathcal{K}_{m,n} &= \\ &\frac{2\pi R_d |T_{r,0}|}{R_d} K_{n,m} \\ \text{or} \\ &\frac{D_r 2\pi R_d}{R_d^3} K_{n,m}, \end{aligned}$$

in the high-stress and low-stress limits, respectively.  $\rho h \pi R_d^2$  is the mass of the drum (in kg), and  $2\pi R_d |T_{r,0}|$  the force tensioning the device at the periphery (in N, equivalent to  $S_z$  for the beam case, see Figs. 1 and 2). Similarly, the flexural rigidity times perimeter  $D_r 2\pi R_d$  replaces the product  $E_z I_z$  of the Euler-Bernoulli modeling. Numerical values for  $M_{n,m}$  and  $K_{n,m}$  are listed in Tab. III. Note that the mass parameters  $M_{n,m}$  obtained in both high-stress and low-stress limits are very close. Resonance frequencies are then given by Eq. (43).

mode $\{n, m\}$	H.S. $C_{n,m}^{(1)}$	H.S. $C_{n,m}^{(2)}$	L.S. $C_{n,m}^{(1)}$	L.S. $C_{n,m}^{(2)}$
$\{0, 0\}$	0.389664	0.389664	0.316669	0.316669
$\{0, 1\}$	0.881992	0.881992	0.851698	0.851698
$\{1, 0\}$	1.139994	0.618625	0.920002	0.630386
$\{1, 1\}$	2.60152	0.671898	2.50136	0.682519
$\{0, 2\}$	1.37954	1.37954	1.34492	1.34492
$\{2, 0\}$	1.62609	1.58811	1.31374	1.62645
$\{1, 2\}$	4.07293	0.692365	3.96830	0.696559
$\{2, 1\}$	3.71904	1.79259	3.55652	1.83054
...	...	...	...	...

TABLE IV: Nonlinear coefficients  $C_{n,m}^{(1,2)}$  computed for the first modes. Left: high-stress (H.S.) and right: low-stress (L.S.). Note the specificity of  $n = 0$  modes (by definition  $C_{0,m}^{(1)} = C_{0,m}^{(2)}$ , no angular dependence of strain/stress).

In Tab. IV we give the stretching  $C_{n,m}^{(1,2)}$  constants (no units) calculated for the first modes. High-stress and low-stress cases are again presented; the obtained numerical values in the two limits are very similar. As an illustrative example, the stretching function  $\epsilon$  calculated for mode  $\{n = 2, m = 1\}$  in the high-stress limit is presented in Fig. 4 (in normalized units).

We finally propose numerical estimates for the nonlinear coefficients written as:

$$\begin{aligned} \tilde{\mathcal{K}}_{n,m} &= + \frac{E_r h 2\pi R_d}{R_d^3} \times \\ &\left[ \frac{C_{n,m}^{(1)} + C_{n,m}^{(2)}}{2} \eta^{(0)}(\nu_r) \tilde{K}_{n,m}^{(1)} + \right. \\ &\left. \frac{C_{n,m}^{(1)} - C_{n,m}^{(2)}}{2} \times \left( \eta_r^{(n)}(\nu_r) \tilde{K}_{n,m}^{(2)} + \eta_\theta^{(n)}(\nu_r) \tilde{K}_{n,m}^{(3)} \right) \right], \end{aligned}$$

where the adimensional  $\tilde{K}_{n,m}^{(1,2,3)}$  are given in Tabs. V and VI (high-stress and low-stress limits respectively).

mode $\{n, m\}$	H.S. $\tilde{K}_{n,m}^{(1)}$	H.S. $\tilde{K}_{n,m}^{(2)}$	H.S. $\tilde{K}_{n,m}^{(3)}$
$\{0, 0\}$	0.779325	X	X
$\{0, 1\}$	1.76398	X	X
$\{1, 0\}$	1.75862	0.352992	-0.0598902
$\{1, 1\}$	3.27341	0.578822	-0.0332539
$\{0, 2\}$	2.75908	X	X
$\{2, 0\}$	3.21421	0.421149	-0.0997277
$\{1, 2\}$	4.76527	0.817227	-0.0230206
$\{2, 1\}$	5.51164	0.607419	-0.0562541
...	...	...	...

TABLE V: Nonlinear Duffing coefficients  $\tilde{K}_{n,m}^{(1,2,3)}$  (no units) computed for the first modes, high-stress (H.S.) limit. Note that  $\tilde{K}_{n,m}^{(1)} = K_{n,m}$  (H.S.), Tab. III. For  $n = 0$  modes,  $\tilde{K}_{0,m}^{(2,3)}$  are irrelevant (X above).

Note the chosen normalization, that matches the Euler-Bernoulli formalism with  $h2\pi R_d$  the cross-section area of the device at the clamp; in the high-stress limit,  $\tilde{K}_{n,m}^{(1)} = K_{n,m}$ .

From Tabs. V and VI, the  $C_{n,m}^{(1,2)}$  values of Tab. IV and the expressions of the functions  $\eta_{r,\theta}^{(n)}(\nu_r)$  [Eqs. (36,37) and subsequent text], one realizes that the geometrical Duffing nonlinear parameter is *dominated by the homogeneous contribution*. As a result,  $\tilde{K}_{n,m}$  is *always positive*, as in the beam case. Finally, one can see that the numerical evaluations of  $\tilde{K}_{n,m}^{(1,2,3)}$  are about twice larger in the

high-stress limit than in the low-stress case. As such, for identical material parameters ( $E_r, \nu_r, \rho$ ) except the biaxial stress  $\sigma_0$  and identical geometry ( $R_d, h$ ), a membrane Duffing nonlinearity  $\tilde{K}_{n,m}$  (H.S.) is approximately *twice larger* than for a plate (L.S.).

mode $\{n, m\}$	L.S. $\tilde{K}_{n,m}^{(1)}$	L.S. $\tilde{K}_{n,m}^{(2)}$	L.S. $\tilde{K}_{n,m}^{(3)}$
$\{0, 0\}$	0.316669	X	X
$\{0, 1\}$	0.851698	X	X
$\{1, 0\}$	0.775194	0.205519	-0.0461452
$\{1, 1\}$	1.59194	0.433603	-0.0299831
$\{0, 2\}$	1.34492	X	X
$\{2, 0\}$	1.47010	0.209512	-0.066682
$\{1, 2\}$	2.33243	0.663581	-0.0213665
$\{2, 1\}$	2.69353	0.388931	-0.0474821
...	...	...	...

TABLE VI: Nonlinear Duffing coefficients  $\tilde{K}_{n,m}^{(1,2,3)}$  (no units) computed for the first modes, low stress (L.S.) limit. For  $n = 0$  modes,  $\tilde{K}_{0,m}^{(2,3)}$  are irrelevant (X above).

---

[1] A. N. Cleland and M. L. Roukes, Fabrication of high frequency nanometer scale mechanical resonators from bulk Si crystals, *Appl. Phys. Lett.* 69, 2653 (1996).

[2] A. N. Cleland, *Foundations of nanomechanics*, Springer (2003).

[3] Silvan Schmid, Luis Guillermo Villanueva, Michael Lee Roukes, *Fundamentals of Nanomechanical Resonators*, Springer (2016).

[4] V. Kara, Y.-I. Sohn, H. Atikian, V. Yakhot, M. Loncar, K. L. Ekinci, Nanofluidics of Single-Crystal Diamond Nanomechanical Resonators, *Nano Letters* 15, 12, 8070-8076 (2015).

[5] K. Jensen, J. Weldon, H. Garcia, A. Zettl, *Nano Lett.* 7, 11, 3508-3511 (2007).

[6] Aneesh Koka and Henry A. Sodano, High-sensitivity accelerometer composed of ultra-long vertically aligned barium titanate nanowire arrays, *Nature Communications* 4, 2682 (2013).

[7] Eric Sage, Marc Sansa, Shawn Fostner, Martial Defoort, Marc Gly, Akshay K. Naik, Robert Morel, Laurent Duraffourg, Michael L. Roukes, Thomas Alava, Guillaume Jourdan, Eric Colinet, Christophe Masselon, Ariel Brenac and Sbastien Hentz, Single-particle mass spectrometry with arrays of frequency-addressed nanomechanical resonators, *Nature Communications* 9, 3283 (2018).

[8] A. D. O'Connell, M. Hofheinz, M. Ansmann, Radoslaw C. Bialczak, M. Lenander, Erik Lucero, M. Neeley, D. Sank, H. Wang, M. Weides, J. Wenner, John M. Martinis and A. N. Cleland, Quantum ground state and single-phonon control of a mechanical resonator, *Nature* 464, 697-703 (2010).

[9] T. A. Palomaki, J. W. Harlow, J. D. Teufel, R. W. Simmonds, K. W. Lehnert, Coherent state transfer between itinerant microwave fields and a mechanical oscillator, *Nature* 495, 210 (2013).

[10] J.-M. Pirkkalainen, S. U. Cho, Jian Li, G. S. Paraoanu, P. J. Hakonen and M. A. Sillanpää, Hybrid circuit cavity quantum electrodynamics with a micromechanical resonator, *Nature* 494, 211 (2013).

[11] H. W. Ch. Postma, I. Kozinsky, A. Husain, and M. L. Roukes, Dynamic range of nanotube- and nanowire-based electromechanical systems, *Appl. Phys. Lett.* 86, 223105 (2005).

[12] R. Almog, S. Zaitsev, O. Shtempluck, and E. Buks, High intermodulation gain in a micromechanical Duffing resonator, *Appl. Phys. Lett.* 88, 213509 (2006).

[13] I. Mahboob and H. Yamaguchi, Bit storage and bit flip operations in an electromechanical oscillator, *Nature Nanotechnology* 3, 275 (2008).

[14] Warner J. Venstra, Hidde J. R. Westra, and Herre S. J. van der Zant, Mechanical stiffening, bistability, and bit operations in a microcantilever, *Appl. Phys. Lett.* 97, 193107 (2010).

[15] M. C. Cross, A. Zumdieck, Ron Lifshitz, and J. L. Rogers, Synchronization by Nonlinear Frequency Pulling, *Phys.*

Rev. Lett. 93, 224101 (2004).

[16] Matthew H. Matheny, Matt Grau, Luis G. Villanueva, Rassul B. Karabalin, M. C. Cross, and Michael L. Roukes, Phase Synchronization of Two Anharmonic Nanomechanical Oscillators, Phys. Rev. Lett. 112, 014101 (2014).

[17] I. Kozinsky, H. W. Ch. Postma, I. Bargatin, and M. L. Roukes, Tuning nonlinearity, dynamic range, and frequency of nanomechanical resonators, Appl. Phys. Lett. 88, 253101 (2006).

[18] N. Kacem, J. Arcamone, F. Perez-Murano and S. Hentz, Dynamic range enhancement of nonlinear nanomechanical resonant cantilevers for highly sensitive NEMS gas/mass sensor applications, J. Micromech. Microeng. 20, 045023 (2010).

[19] Lily L. Li, Pavel M. Polunin, Suguang Dou, Oriel Shoshani, B. Scott Strachan, Jakob S. Jensen, Steven W. Shaw, and Kimberly L. Turner, Tailoring the nonlinear response of MEMS resonators using shape optimization, Appl. Phys. Lett. 110, 081902 (2017).

[20] R. Lifshitz and M.C. Cross, in *Reviews of Nonlinear Dynamics and Complexity*, Ed. by H. G. Schuster, Wiley-VCH (2008).

[21] M. Defoort, *Non-linear dynamics in nano-electromechanical systems at low temperatures*, PhD thesis, Université de Grenoble (16/12/2014).

[22] E. Collin, Yu. M. Bunkov, and H. Godfrin, Addressing geometric nonlinearities with cantilever microelectromechanical systems: Beyond the Duffing model, Phys. Rev. B 82, 235416 (2010).

[23] K. J. Lulla, R. B. Cousins, A. Venkatesan, M. J. Patton, A. D. Armour, C. J. Mellor and J. R. Owers-Bradley, Nonlinear modal coupling in a high-stress doubly-clamped nanomechanical resonator, New Journal of Physics 14, 113040 (2012).

[24] M. H. Matheny, L. G. Villanueva, R. B. Karabalin, J. E. Sader, and M. L. Roukes, Nonlinear Mode-Coupling in Nanomechanical Systems, Nano Lett. 13, 1622 (2013).

[25] Olivier Maillet, Xin Zhou, Rasul Gazizulin, Ana Maldonado Cid, Martial Defoort, Olivier Bourgeois, Eddy Collin, Non-linear Frequency Transduction of Nano-mechanical Brownian Motion, Phys. Rev. B 96, 165434 (2017).

[26] B. Yurke, D.S. Greywall, A.N. Pargellis, P.A. Bush, Theory of amplifier-noise evasion in an oscillator employing a nonlinear resonator, Phys. Rev. A 51, 4211 (1995).

[27] Mohammad Amin Rashidifar, *Nonlinear Vibrations of Cantilever Beams and Plates*, Hamburg, Anchor Academic Publishing (2015).

[28] M. Amabili, *Nonlinear Vibrations and Stability of Shells and Plates*, Cambridge University Press (2008).

[29] G. W. Vogl, A. H. Nayfeh, A reduced model for electrically actuated clamped circular plates, Journal of Micromechanics and Microengineering 315, 684-690, (2005).

[30] G. W. Vogl, A. H. Nayfeh, Primary resonance excitation of electrically actuated clamped circular plates, Nonlinear Dynamics 47, 181-192, (2007).

[31] B. Sajadi, F. Alijani, D. Davidovikj, J. Goosen, P. G. Steeneken, F. V. Keulen, Experimental characterization of graphene by electrostatic resonance frequency tuning, Journal of Applied Physics 122, 234302, (2017).

[32] L.D. Landau and E.M. Lifshitz, *Theory of elasticity*, Butterworth-Heinemann, Oxford 3rd Ed. (1986).

[33] D. Davidovikj, F. Alijani, S.J. Cartamil-Bueno, H.S.J. van der Zant, M. Amabili P.G. Steeneken, Nonlinear dynamic characterization of twodimensional materials, Nature Comm. 8, 1253 (2017).

[34] Fan Yang, Felix Rochau, Jana S. Huber, Alexandre Brieussel, Gianluca Rastelli, Eva M. Weig, and Elke Scheer, Spatial Modulation of Nonlinear Flexural Vibrations of Membrane Resonators, Phys. Rev. Lett. 122, 154301 (2019).